MOF Catalysts Hot Paper

How to cite: *Angew. Chem. Int. Ed.* **2021**, *60*, 24312–24317
International Edition: doi.org/10.1002/anie.202111893
German Edition: doi.org/10.1002/ange.202111893

Functional Porphyrinic Metal–Organic Framework as a New Class of Heterogeneous Halogen-Bond-Donor Catalyst

*Weijie Zhang, Ayman Nafady, Chuan Shan, Lukasz Wojtas, Yu-Sheng Chen, Qigan Cheng, X. Peter Zhang, and Shengqian Ma**

Abstract: *Biomimetic metal-organic frameworks have attracted great attention as they can be used as bio-inspired models, allowing us to gain important insights into how large biological molecules function as catalysts. In this work, we report the synthesis and utilization of such a metal-metalloporphyrin framework (MMPF) that is constructed from a custom-designed ligand as an efficient halogen bond donor catalyst for Diels–Alder reactions under ambient conditions. The implementation of fabricated halogen bonding capsule as binding pocket with high-density C−Br bonds enabled the use of halogen bonding to facilitate organic transformations in their three-dimensional cavities. Through combined experimental and computational studies, we showed that the substrate molecules diffuse through the pores of the MMPF, establishing a host-guest system via the C−Br···π interaction. The formation of halogen bonds is a plausible explanation for the observed boosted catalytic efficiency in Diels–Alder reactions. Moreover, the unique capability of MMPF highlights new opportunities in using artificial non-covalent binding pockets as highly tunable and selective catalytic materials.*

Introduction

Non-covalent interactions can be considered as a weak electromagnetic interaction either between two molecules or within a molecule, without sharing of electrons. These weak interactions ($\approx$0.5–3 kcal mol^{-1}), such as hydrophobic effect, van der Waals forces, halogen bonding and electrostatic interactions, play a vital role in catalysis, crystal engineering, self-assembly, drug molecule design, molecular biology, molecular recognition, etc.[1]

It is well known that non-covalent interactions can easily lower the free energy as the substrate-catalyst (S-C) species forms and then approaches the transition state, which partially offsets for the energetic uptake and cost that is required to form the activated S-C complex and thereby leads to enhanced catalysis.[2] These catalysts generally offer mild but selective activation of a specific functional group as a result of their weak S-C interactions. In particular, halogen bonding interactions are widely encountered in biological systems (Scheme 1 a). In nature, halogen-bond plays vital roles in the biology of thyroid hormones, from its recognition by receptors, to the iodine salvage during its catabolism and subsequent anabolism.[3] The formation of a relatively pos-

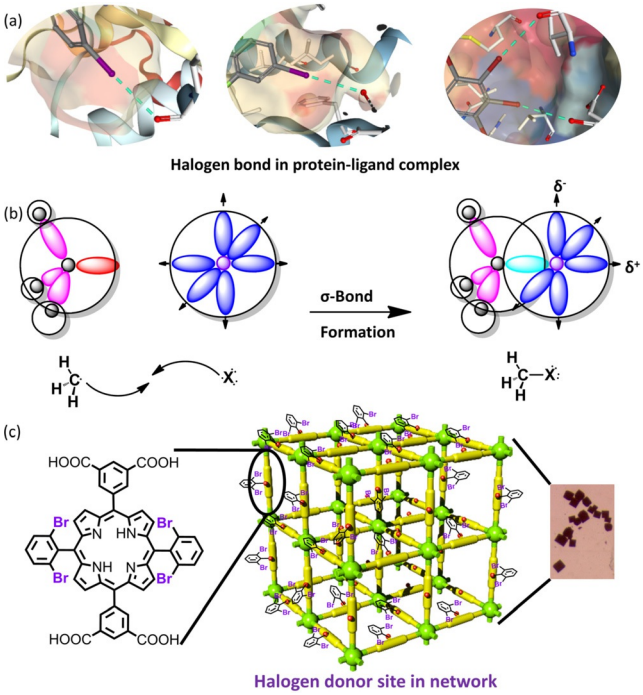

Scheme 1. a) Halogen-bond formation in PDB 3DV3, 3DY7 and 3KXH between the backbone carbonyl oxygen and the halogen atom. b) The formation of the sigma hole: The covalent bond (C−X) between the halogen (σ-bond, green) pairs and the carbon atom, an electron from the carbon atom with one from the halogen atom. c) 5,15-*bis*(3,5-dicarboxyphenyl)-10,20-*bis*(2,6-dibromophenyl)porphyrin (H_4dcdbp) ligand in this work, a high density of halogen-donor sites in the MMPF network and the microscope images of Mg-MMPF-3.

[*] Dr. W. Zhang, Prof. Dr. S. Ma
Department of Chemistry, University of North Texas
Denton, TX 76203 (USA)
E-mail: Shengqian.Ma@unt.edu
Prof. Dr. A. Nafady
Department of Chemistry, College of Science, King Saud University
Riyadh 11451 (Saudi Arabia)
C. Shan, Dr. L. Wojtas, Dr. Q. Cheng
Department of Chemistry, University of South Florida
4202 East Fowler Avenue, Tampa, FL 33620 (USA)
Dr. Y.-S. Chen
ChemMatCARS, Center for Advanced Radiation Sources, University of Chicago
9700 S. Cass Avenue, Argonne, IL 60439 (USA)
Prof. Dr. X. P. Zhang
Department of Chemistry, Merkert Chemistry Center, Boston College
Chestnut Hill, MA 02467 (USA)
Supporting information and the ORCID identification number(s) for the author(s) of this article can be found under: https://doi.org/10.1002/anie.202111893.

itively charged region, called "sigma hole" (σ hole) can manifest the anisotropic distribution of electronic charge density around the halogen atom (Scheme 1b). The existence of the electro-positive σ hole allows for the non-covalent interactions with the lone pair electrons of other electronegative systems in the vicinity of the halogen atom. The investigation of the σ hole, halogen bonding interactions and their subsequent application has been the subject of extensive studies in the past decade.[4] For example, iodine trichloride (ICl_3) takes part in the ring-opening polymerization of L-lactide with the aid of 11-bromo-1-undecanol;[5] the carbonyl activation of L-lactide through halogen bonding was further demonstrated by NMR and FT-IR spectroscopy studies. By far there have been only a few reports on halogen bond donor catalysts,[6] and such research area remains largely unexplored particularly in the heterogeneous catalysis field.

Enzymes feature sophisticated assembled binding pockets able to recognize the specific substrates via multiple non-covalent interactions, which not only enhance the reaction rate but also render regio- and stereo-selectivity in the reactions. Recently, biomimetic metal-organic frameworks (MOFs) are of considerable interest as they can be readily employed as models for bio-mimicking in catalysis, thus helping to gain deep insights into how large biological molecules function.[7] In this respect, the channels or cavities in MOFs can serve as "pockets" or "molecular flasks" that resemble those of the active site machinery of enzymes.[8] In particular, there has been an escalating interest in utilizing bio-ligands for the construction of biomimetic MOFs as they have several advantages such as multiple metal binding sites, simple synthetic pathways and structural diversity. The incorporation of metalloporphyrins,[9] corrole[10] or phthalocyanine[11] into MOFs has been successfully demonstrated to construct the artificial metalloenzymes. A family of metal-metalloporphyrin frameworks (MMPFs) as catalytic pockets have been explored for their desirable properties since 2011 by our research group.[12] Multiporphyrinic pocket compounds with elegant structures have well-defined inner cavities with enhanced rigidity, hydrophobic properties and large space to favor efficient guest binding. By far, most biomimetic MOF studies have been focused on the imitation of the metal sites and coordination environments that exist in enzymes. Recently, the concept of designing biomimetic pockets with non-covalent bond sites has emerged as a promising approach for developing new mild yet selective catalytic transformations. However, the incorporation of various types of non-covalent intermolecular interactions for MOFs-based catalysis has been barely reported,[13] which necessitates wide exploration.

In recent years, Diels–Alder reactions,[14] also known as the [4+2] cycloaddition reactions, are one of the most fascinating cornerstone transformations in organic chemistry. Diels–Alder reactions have been widely used for the synthesis of natural products and biologically active compounds. As a group of thermally promoted reactions, Diels–Alder reactions usually occur in high boiling solvents and at elevated temperatures. Such demanding reaction conditions can be alleviated by the rational design of porous material-based catalyst that can confine the reactants in their nano-space, which also affects the selectivity of Diels–Alder reactions.[15] The utilization of non-covalent interactions such as C–H···π interactions and π···π interactions, to promote Diels–Alder reactions under ambient conditions have recently been reported in a few homogeneous systems.[13a,16] We speculate that creating artificial non-covalent binding pockets within highly porous MOFs can facilitate the Diels–Alder reactions under ambient conditions in heterogeneous systems with high selectivity and efficient conversion.

In this contribution, we show that incorporating C-Br bonds into the porphyrin ligand allows for the construction of MMPF as halogen bond donor catalyst in a heterogeneous manner (Scheme 1c), which, to the best of our knowledge, represents the first example showing the significant enhancement of catalytic performance via formed halogen bonding. In this context, C–Br···π interaction has been deemed as a positive effect on nucleophilicity,[17] as it adds electron density to the π system, thereby satisfying the electron demand of Diels–Alder reaction.[13a,16] We therefore envision that resultant MMPF exhibits high catalytic activity for Diels–Alder reactions under ambient conditions. In addition, the highly crystalline nature of MMPF can help to understand the host-guest interactions during the catalysis, thus offering an excellent platform for studying the catalytic mechanisms. Moreover, MMPF can encapsulate the aromatic reactants and reorganize them in its confined space via halogen bonding, which could lead to high-yield products with a rapid reaction rate at mild temperatures.

Results and Discussion

5,15-*bis*(3,5-dicarboxyphenyl)-10,20-*bis*(2,6-dibromophenyl)porphyrin (H_4dcdbp) was synthesized using the procedures reported previously (Scheme S1–S3, Figure S1–S14, see the Supporting Information for details).[12c] A solvothermal reaction between H_4dcdbp and $MgCl_2{\cdot}6H_2O$ in dimethylacetamide (DMA) and methanol at 100 °C afforded cube-shaped, purple crystals of Mg-MMPF-3 (≈70% yield, as shown in Figure S15), which has an empirical formula of $[Mg_2(\mu_2\text{-}H_2O)(H_2O)_4](dcdbp)(CH_3OH)_{12}(DMA)_{12}$ as determined by X-ray crystallography analysis, elemental analysis, and thermogravimetric analysis. Single-crystal X-ray diffraction studies revealed that Mg-MMPF-3 crystallizes in the space group *R*-3, which is different from the space group of Co-MMPF-3 (Table S1, Figure S16 and S17).[12c]

Mg-MMPF-3 features three different polyhedral cages: the cubohemioctahedron (Cage 1) with a window size of ≈6.0 Å and the inner dimensions of ≈7 Å (Figure 1a); the truncated tetrahedron (Cage 2) with a window size of ≈19 Å and the dibromophenyl moieties residing in the inner space of the cage (Figure 1b); the truncated octahedron (Cage 3) with a window size of ≈10 Å and the inner dimensions of ≈26 Å (Figure 1c). In both Cage 2 and Cage 3, the dcdbp linkers occupy the polyhedron edges. Cage 3 in Mg-MMPF-3 possesses twenty-four C–Br bonds that orient towards the cage center with a density of ≈7 (C-Br)/nm^3 (Figure S18). The three different types of polyhedral cage are interconnected as shown in Figure 1d, and Mg-MMPF-3 has a total

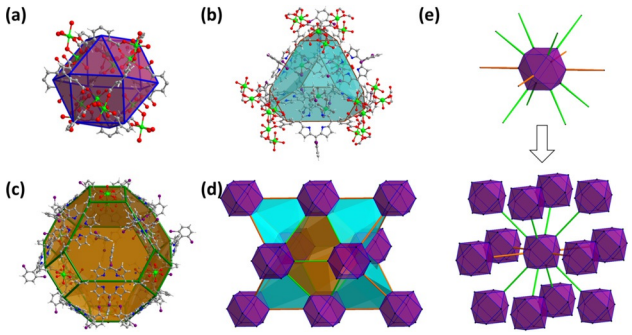

Figure 1. The three different types of polyhedral cages present in Mg-MMPF-3: a) the cubohemioctahedron, b) the truncated tetrahedron, and c) the truncated octahedron. d), e) 3D structure of Mg-MMPF-3 showing how its polyhedral cages are connected into the network.

potential solvent-accessible volume of ≈60% as calculated from PLATON. Mg-MMPF-3 is based upon $Mg_2(\mu_2\text{-}H_2O)(H_2O)_4(COO)_4$ building blocks (Figure S19) that afford the cubohemioctahedral second building blocks (SBBs, Figure 1a). The SBBs serve as the 12-connected nodes in the resultant ***fcu*** topology framework (Figure 1e). The FT-IR spectra of dcdbp-$COOCH_3$, H_4dcdbp, and Mg-MMPF-3 are shown in Figure S20. It can be observed that porphyrin ligand presents two absorption peaks at around 1710 and 1207 cm^{-1}, which correspond to the symmetrical and asymmetric stretching vibrations of carboxylic acid, respectively. As for MMPFs, the appearance of two main absorption peaks at around 1568 and 1390 cm^{-1} is mainly due to the coordination Mg^{2+} with deprotonated carboxylic group.

The powder *x*-ray diffraction (PXRD) patterns for the bulk samples of Mg-MMPF-3 matched well the calculated ones from the single crystal CIF file (Figure S21). The stability was also tested by dispersing the Mg-MMPF-3 samples in different solvents, such as DCM, methanol, acetone and ethanol. Thermogravimetric analysis (TGA) of freshly prepared Mg-MMPF-3 revealed ≈30% weight loss after heating to 125 °C (Figure S22). Another weight loss was observed starting at ≈160 °C, which was ascribed to the loss of DMA guests. Similarly, the PXRD patterns of the heated material indicated the loss of crystallinity after heated above 150 °C. We accomplished the sample activation by exchanging DMA with methanol or ethanol over a period of 3 days. The standard thermal activation proved successful in the removal of all DMA guest molecules. ICP-OES and Energy-dispersive X-ray spectroscopy (EDS) confirmed the proposed metal ratios (Figure S23). X-ray photoelectron spectroscopy (XPS) was employed to analyze the elemental compositions of Mg-MMPF. The full survey of Mg-MMPF confirms the existence of C, O, N, Mg elements (Figure S24). The high-resolution XPS of Mg2p is shown in Figure S25, suggesting the presence of Mg^{2+}. Furthermore, the permanent porosity of Mg-MMPF-3 was confirmed by both CO_2 adsorption (Figure S26) and N_2 adsorption (Figure S27), which revealed a surface of ≈670 $m^2 g^{-1}$.

Structure analysis revealed that the Cage 3 is composed of the electron-rich C-Br bonds of the ligand, which could facilitate the encapsulation of aromatic reactants through C-Br···π interactions. This promoted us to examine Mg-MMPF-3 as a heterogeneous halogen bond donor catalyst for Diels–Alder reactions. When 9-hydroxymethylanthracene (0.05 mmol) and N-phenylmaleimide (0.05 mmol) were added to ethanol in the presence of Mg-MMPF-3 (10 mg) at room temperature and 1 bar, the adduct formation yield was 90% after 4 h and >99% after 7 h, as estimated from combined GC (Figure S28) and NMR analyses (Figure S29–S31). We compared ethanol with two less polar solvents CH_3CN and isopropanol and no significant changes in the yield and reaction rate were observed among the three solvents (Figure S32). By contrast, only 25% product was isolated under the same reaction conditions in the presence of H_4dcdbp, which was comparable to the blank control reaction (i.e. without any catalyst) with a yield of 23%. Single-crystal X-ray diffraction studies revealed that the H_4dcdbp molecules were closely packed through the halogen bonding interaction thus leading to the aggregation-caused catalyst deactivation (Figure S33). This result highlighted the ordered distribution of dibromophenyl moieties into 3D nanospace of MOF as a prerequisite to achieve high catalysis efficiency in Mg-MMPF-3. As shown in Figure S29, there was no chemical shift around 4.5 ppm, which meant that the reaction occurred at the 9,10-position of anthracene to give 9,10-adduct, rather than at 1,4-position to 1,4-adduct,[15a] thereby indicating the high selectivity of Mg-MMPF-3 for Diels–Alder reactions.

To investigate the potential contribution from Mg^{II} in the $Mg_2(\mu_2\text{-}H_2O)(H_2O)_4(COO)_4$ building blocks to the catalysis performance of Mg-MMPF-3, control experiments were conducted for the reaction in the presence of $MgCl_2{\cdot}6H_2O$. No significant increase in the yield was observed as compared with the blank control reaction, meaning negligible contribution from $Mg_2(\mu_2\text{-}H_2O)(H_2O)_4(COO)_4$ building blocks. This result thereby further indicated the important contribution from the dibromophenyl moieties of dcdbp ligands which reside on the pore walls of Mg-MMPF-3, to facilitating Diels–Alder reactions in a heterogeneous manner.

To highlight the role of non-covalent halogen bonding interactions in promoting Diels–Alder reactions, we compared Mg-MMPF-3 with PCN-221[18] (Figure S34) and MMPF-5[12b] (Figure S35), porphyrinic MOFs which feature similar cavities to Mg-MMPF-3 but possesses C–H bonds instead of C-Br bonds on the pore walls. As shown in Figure 2, Mg-MMPF-3 is a more active catalyst than PCN-221 and MMPF-5 for Diels–Alder reaction (99% yield at 8 h vs. 80% yield and 62% yield). Given their structural similarity, we ascribed the higher catalytic activity of Mg-MMPF-3 in comparison with PCN-221 and MMPF-5 mainly to the existence of densely populated C-Br bonds in the former, wherein the C–Br···π interactions can better promote the Diels–Alder reaction through than the C–H···π interactions in PCN-221. We further compared the catalytic performance of Co-MMPF-3, which was reported by our group. Figure 2b revealed that Co-MMPF-3 converted 95% of substrate after 8 h, which is comparable to Mg-MMPF-3. Control experiments were also conducted on some more simple and accessible halogen-decorated or non-halogenated MOFs (Figure S36–S38, see the supporting information for more synthetic details). As shown in Figure S39, much lower

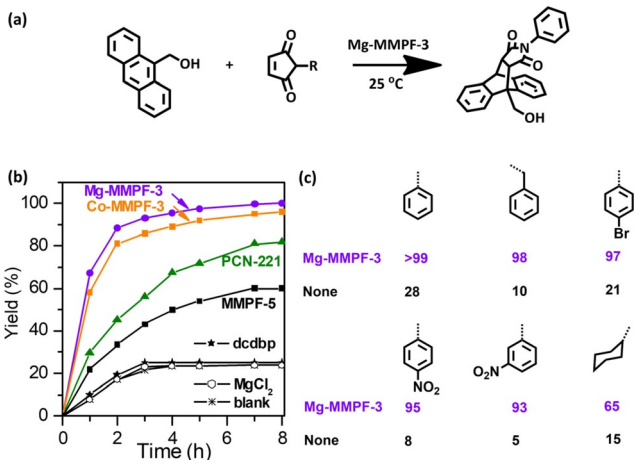

Figure 2. a) Diels–Alder reactions of N-substituted maleimides and 9-hydroxyanthracene catalyzed by Mg-MMPF-3. b) Yield versus time curves for the Diels–Alder reaction at room temperature and 1 bar. c) The yields for a variety of maleimide derivatives catalyzed by Mg-MMPF-3 and without catalyst (blank).

activities were observed for those non-porphyrinic halogen-decorated MOFs with the 2-hour yields of 28%, 20%, and 26% for Br-MIL-101, Br-UiO-66, and Br-ZIF-7 respectively, which, however, were comparable with their non-halogenated counterparts MIL-101 (23%), UiO-66 (20%) and ZIF-7 (21%). These results further highlighted the strong affinities of porphyrin ligands to substrate molecules. The examined catalyst could be separated by easy filtration and washed several times with methanol. No detectable leaching of metal ion in the reaction solution was observed after the catalyst removal by filtration. Mg-MMPF-3 could be recycled eight times without a significant decrease in catalytic performance (Figure S40).

We next investigated the substrate scope to assess whether Mg-MMPF-3 could efficiently catalyze different N-substituents maleimide derivatives. A variety of N-substituents maleimide derivatives, including N-phenyl, N-benzyl, N-(*p*-nitro)phenyl, N-(*p*-bromo)phenyl, N-cyclohexyl, N-(*m*-nitro)phenyl were used to react with 9-hydroxymethylanthracene. All products were purified using column chromatography and further characterized by ^{1}H and ^{13}C NMR spectroscopy (Figure S41–S54, see the supporting information for full details). Poly-aromatic N-maleimides like N-(*p*-Bromophenyl)maleimide, N-Benzylmaleimide, N-(*m*-Nitrophenyl)-maleimide and N-(*p*-Nitrophenyl)maleimide are generally less reactive; however, remarkably increased yields were obtained in the presence of Mg-MMPF-3 (Figure 2b). A much lower yield (65%) was observed for N-cyclohexylmaleimide as compared with the phenyl maleimides, which can be attributed to the weaker electron delocalization owing to the presence of the aliphatic cyclohexyl group. The above catalysis results suggest that the non-covalent interactions between the C-Br bonds and the π systems of the highly electron delocalized poly-aromatic reactants can efficiently promote Diels–Alder reactions thus affording high catalytic activity for Mg-MMPF-3.

As the encapsulation of the reactants is the critical step of the three-step catalytic mechanism, including encapsulation, reorganization and adduct formation, we investigated whether the catalysis occurred within the pores or on the surface of Mg-MMPF-3. Therefore, encapsulation experiments were conducted by adding the Mg-MMPF-3 and other control samples to the 9-hydroxymethylanthracene ethanol solution (Figure S55 and S56).[16] It can be observed that the absorbance intensity of the 9-hydroxymethylanthracene solution decreased, indicating that 9-hydroxymethylanthracene can be trapped within the cavities of the Mg-MMPF-3. From the absorption spectral profile change, the concentration of 9-hydroxymethylanthracene in the Mg-MMPF-3 is approximately fifty-three times greater than that in bulk solution after 8 h.

To understand how non-covalent interactions promote Diels–Alder reactions in Mg-MMPF-3, we adopted a simplified system with focus on investigating the affinities of porphyrin ligands featuring C–X bond (X = Br or H) donors to anthracene molecules through combined studies of crystal structure analysis, computational calculations, and UV/Vis spectroscopy. It's been previously reported that tetraphenylporphyrin (TPP) could be co-crystallized with anthracene.[19] After a careful analysis of the co-crystal structure, we found that the two different chemical entities aggregates in a crystalline lattice mainly through the C–H···π interactions (Figure S57) with anthracene located above one half of the porphyrin ring, rather than above the phenyl rings of TPP. Based on the structure of the TPP-anthracene co-crystal, we built two systems in order to rationalize the non-covalent interactions via quantum chemical calculations: TPP + anthracene and dcdbp + anthracene. The calculated interaction energy between porphyrin and anthracene was found to correlate strongly with the type of non-covalent bond. That is, the C–X bond (X = H or Br) has substantial effects, as apparent from the potential energy curves regarding the C–X···π distance. The C-Br bond affords favorable interaction with anthracene in a broad *d*(C–Br···π) range (Figure S58). In contrast, the intermolecular interaction already becomes repulsive at a rather large C–H···π distance in TPP···anthracene, which may hamper efficient electron delocalization during catalysis.

In order to gain insight into the role of C–Br···π in promoting Diels–Alder reactions, UV/Vis spectra were measured for the mixture of TPP/9-hydroxymethylanthracene and H_4dcdbp/9-hydroxymethylanthracene (Figure S59–S61, Figure S60 for TPP and Figure S61 for H_4dcdbp). We did not observe noticeable change in the peak associated with the π-π* transition of 9-hydroxymethylanthracene. This can be aligned to the energy level increase for both π orbitals and π* orbitals without changing the ΔE(π-π*) value (black lines to purple lines in Figure 3a). Red shifts were observed for peaks associated with *n*-π* transition of 9-hydroxymethylanthracene in both solutions. As shown in Figure S62, these shifts were more profound for the H_4dcdbp/9-hydroxymethylanthracene system, which indicate that the C–Br···π interaction, acting as an electron donating group, increases electronic density of conjugated system and then accordingly narrows the *n*-π* transition from alcoholic hydroxyl group. The ΔE_1

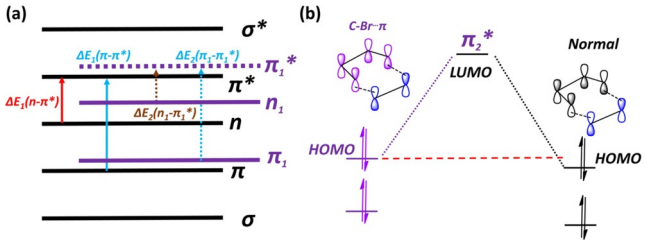

Figure 3. A scalar quantization of the Diels–Alder reaction catalyzed by halogen bond. a) The orbitals by the black or purple lines represent the energy levels of anthracene molecular without or with the C–Br···π interactions. b) The highest occupied molecular orbital (HOMO, π_1) of 9-hydroxymethylanthracene and the lowest unoccupied molecular orbital (LUMO, π_2*) of the electron-deficient N-substituted maleimide; the black or purple lines represent the HOMO of anthracene molecular without or with the C–Br···π interactions.

(n-π*) value is higher than the ΔE_2 (n_1-π_1*) value based on the observed red shift in the spectrum. Under the influence of the halogen bond interactions, the n_1 orbitals become closer to the π_1* orbitals from a scalar quantization. These features should be taken into account when determining the HOMO–LUMO gap. For the electron demand Diels–Alder reaction, the HOMO–LUMO gap (HOMO for the electron-rich 9-hydroxymethylanthracene's π_1 and LUMO for the electron-deficient N-substituted maleimide's π_2*) was reduced due to the halogen bonding as shown in Figure 3b. A smaller HOMO–LUMO energy gap suggests a lower activation energy thus to favor the Diels–Alder reaction. Hence, based on those above results, it can be concluded the C–Br···π interaction has a positive effect on the nucleophilicity as it adds electron density to the π system to satisfy the electron demand Diels–Alder reaction thereby leading to boosted catalytic performance as observed in Mg-MMPF-3.

Conclusion

In summary, we showcased the creation of artificial non-covalent binding pocket in MOF by constructing a metal-metalloporphyrin framework (MMPF) that is based upon a custom-designed porphyrin ligand featuring C–Br bonds. The constructed MMPF demonstrated excellent catalysis performance for Diels–Alder reactions under ambient conditions, which were promoted by C–Br···π interaction that can reduce the HOMO–LUMO energy gap of the two reactants. Our work not only advances functional porphyrinic MOF as a new class of heterogeneous halogen bond donor catalyst, but also contributes a new approach to mimic enzyme system for highly efficient and selective catalysis.

Acknowledgements

The authors acknowledge the Robert A. Welch Foundation (B-0027) for financial support of this work. The authors also extended their sincere appreciation to Researchers Supporting Program project no (RSP-2021/79) at King Saud University, Riyadh, Saudi Arabia for partially funding this work (A.N.). NSF's ChemMatCARS Sector 15 is supported by the Divisions of Chemistry (CHE) and Materials Research (DMR), National Science Foundation, under Grant Number NSF/CHE-1834750. Use of the Advanced Photon Source, an Office of Science User Facility operated for the U.S. Department of Energy (DOE) Office of Science by Argonne National Laboratory, was supported by the U.S. DOE under Contract No. DE-AC02-06CH11357.

Conflict of Interest

The authors declare no conflict of interest.

Keywords: biomimetic catalysis · halogen-bond donor · metal–organic frameworks (MOFs) · non-covalent interactions · porphyrins

[1] a) B. Moulton, M. J. Zaworotko, *Chem. Rev.* **2001**, *101*, 1629–1658; b) S. J. Benkovic, S. Hammes-Schiffer, *Science* **2003**, *301*, 1196–1202; c) F. Biedermann, H. J. Schneider, *Chem. Rev.* **2016**, *116*, 5216–5300; d) A. J. Kirby, *Angew. Chem. Int. Ed. Engl.* **1996**, *35*, 706–724; *Angew. Chem.* **1996**, *108*, 770–790; e) C. B. Aakeröy, K. R. Seddon, *Chem. Soc. Rev.* **1993**, *22*, 397–407; f) H. J. Schneider, *Angew. Chem. Int. Ed.* **2009**, *48*, 3924–3977; *Angew. Chem.* **2009**, *121*, 3982–4036.

[2] A. J. Neel, M. J. Hilton, M. S. Sigman, F. D. Toste, *Nature* **2017**, *543*, 637–646.

[3] a) M. R. Scholfield, C. M. Zanden, M. Carter, P. S. Ho, *Protein Sci.* **2013**, *22*, 139–152; b) D. Manna, G. Mugesh, *J. Am. Chem. Soc.* **2012**, *134*, 4269–4279; c) P. M. McTamney, S. E. Rokita, *J. Am. Chem. Soc.* **2009**, *131*, 14212–14213.

[4] a) G. Cavallo, P. Metrangolo, R. Milani, T. Pilati, A. Priimagi, G. Resnati, G. Terraneo, *Chem. Rev.* **2016**, *116*, 2478–2601; b) J. Matern, N. Baumer, G. Fernandez, *J. Am. Chem. Soc.* **2021**, *143*, 7164–7175.

[5] O. Coulembier, F. Meyer, P. Dubois, *Polym. Chem.* **2010**, *1*, 434–437.

[6] a) M. D. Perera, C. B. Aakeröy, *New J. Chem.* **2019**, *43*, 8311–8314; b) I. Kazi, S. Guha, G. Sekar, *Org. Lett.* **2017**, *19*, 1244–1247; c) J. P. Gliese, S. H. Jungbauer, S. M. Huber, *Chem. Commun.* **2017**, *53*, 12052–12055; d) D. Bulfield, S. M. Huber, *Chem. Eur. J.* **2016**, *22*, 14434–14450; e) S. H. Jungbauer, S. M. Walter, S. Schindler, L. Rout, F. Kniep, S. M. Huber, *Chem. Commun.* **2014**, *50*, 6281–6284.

[7] a) K. Chen, C.-D. Wu, *Coord. Chem. Rev.* **2019**, *378*, 445–465; b) M. Zhang, Z.-Y. Gu, M. Bosch, Z. Perry, H.-C. Zhou, *Coord. Chem. Rev.* **2015**, *293–294*, 327–356; c) S. L. Anderson, K. C. Stylianou, *Coord. Chem. Rev.* **2017**, *349*, 102–128.

[8] a) T. He, Z. Huang, S. Yuan, X.-L. Lv, X.-J. Kong, X. Zou, H.-C. Zhou, J.-R. Li, *J. Am. Chem. Soc.* **2020**, *142*, 13491–13499; b) Y. Chen, S. Ma, *Dalton Trans.* **2016**, *45*, 9744–9753; c) Z.-B. Fang, T.-T. Liu, J. Liu, S. Jin, X.-P. Wu, X.-Q. Gong, K. Wang, Q. Yin, T.-F. Liu, R. Cao, H.-C. Zhou, *J. Am. Chem. Soc.* **2020**, *142*, 12515–12523; d) X. Lian, Y. Fang, E. Joseph, Q. Wang, J. Li, S. Banerjee, C. Lollar, X. Wang, H. C. Zhou, *Chem. Soc. Rev.* **2017**, *46*, 3386–3401; e) D. Feng, T. F. Liu, J. Su, M. Bosch, Z. Wei, W. Wan, D. Yuan, Y. P. Chen, X. Wang, K. Wang, X. Lian, Z. Y. Gu, J. Park, X. Zou, H. C. Zhou, *Nat. Commun.* **2015**, *6*, 5979–5987; f) P. Li, J. A. Modica, A. J. Howarth, E. Vargas L, P. Z. Moghadam, R. Q. Snurr, M. Mrksich, J. T. Hupp, O. K. Farha, *Chem* **2016**, *1*, 154–169; g) V. Lykourinou, Y. Chen, X. S. Wang, L. Meng, T. Hoang, L. J. Ming, R. L. Musselman, S. Ma, *J. Am. Chem. Soc.* **2011**, *133*, 10382–10385; h) J. Pang, Z. Di, J.-S. Qin,

S. Yuan, C. T. Lollar, J. Li, P. Zhang, M. Wu, D. Yuan, M. Hong, H.-C. Zhou, *J. Am. Chem. Soc.* **2020**, *142*, 15020 – 15026; i) Y. Quan, Y. Song, W. Shi, Z. Xu, J. S. Chen, X. Jiang, C. Wang, W. Lin, *J. Am. Chem. Soc.* **2020**, *142*, 8602 – 8607.

[9] a) M. O. Cichocka, Z. Z. Liang, D. W. Feng, S. Back, S. Siahrostami, X. Wang, L. Samperisi, Y. J. Sun, H. Y. Xu, N. Hedin, H. Q. Zheng, X. D. Zou, H. C. Zhou, Z. H. Huang, *J. Am. Chem. Soc.* **2020**, *142*, 15386 – 15395; b) Y. Bai, Y. Dou, L. H. Xie, W. Rutledge, J. R. Li, H. C. Zhou, *Chem. Soc. Rev.* **2016**, *45*, 2327 – 2367; c) D. Feng, Z. Y. Gu, J. R. Li, H. L. Jiang, Z. Wei, H. C. Zhou, *Angew. Chem. Int. Ed.* **2012**, *51*, 10307 – 10310; *Angew. Chem.* **2012**, *124*, 10453 – 10456; d) W. Morris, B. Volosskiy, S. Demir, F. Gandara, P. L. McGrier, H. Furukawa, D. Cascio, J. F. Stoddart, O. M. Yaghi, *Inorg. Chem.* **2012**, *51*, 6443 – 6445; e) D. Feng, Z. Y. Gu, Y. P. Chen, J. Park, Z. Wei, Y. Sun, M. Bosch, S. Yuan, H. C. Zhou, *J. Am. Chem. Soc.* **2014**, *136*, 17714 – 17717; f) H. L. Jiang, D. Feng, K. Wang, Z. Y. Gu, Z. Wei, Y. P. Chen, H. C. Zhou, *J. Am. Chem. Soc.* **2013**, *135*, 13934 – 13938; g) Y. Keum, S. Park, Y.-P. Chen, J. Park, *Angew. Chem. Int. Ed.* **2018**, *57*, 14852 – 14856; *Angew. Chem.* **2018**, *130*, 15068 – 15072; h) L. Feng, K.-Y. Wang, E. Joseph, H.-C. Zhou, *Trends Chem.* **2020**, *2*, 555 – 568.

[10] Y. Zhao, S. Qi, Z. Niu, Y. Peng, C. Shan, G. Verma, L. Wojtas, Z. Zhang, B. Zhang, Y. Feng, Y. S. Chen, S. Ma, *J. Am. Chem. Soc.* **2019**, *141*, 14443 – 14450.

[11] R. Matheu, E. Gutierrez-Puebla, M. A. Monge, C. S. Diercks, J. Kang, M. S. Prevot, X. Pei, N. Hanikel, B. Zhang, P. Yang, O. M. Yaghi, *J. Am. Chem. Soc.* **2019**, *141*, 17081 – 17085.

[12] a) Y. Chen, T. Hoang, S. Ma, *Inorg. Chem.* **2012**, *51*, 12600 – 12602; b) X.-S. Wang, M. Chrzanowski, L. Wojtas, Y.-S. Chen, S. Ma, *Chem. Eur. J.* **2013**, *19*, 12187 – 12187; c) L. Meng, Q. Cheng, C. Kim, W. Y. Gao, L. Wojtas, Y. S. Chen, M. J. Zaworotko, X. P. Zhang, S. Ma, *Angew. Chem. Int. Ed.* **2012**, *51*, 10082 – 10085; *Angew. Chem.* **2012**, *124*, 10229 – 10232; d) X. S. Wang, M. Chrzanowski, C. Kim, W. Y. Gao, L. Wojtas, Y. S. Chen, X. P. Zhang, S. Ma, *Chem. Commun.* **2012**, *48*, 7173 – 7175.

[13] a) B. Gole, A. K. Bar, A. Mallick, R. Banerjee, P. S. Mukherjee, *Chem. Commun.* **2013**, *49*, 7439 – 7441; b) X. P. Zhang, Z. J. Zhang, J. Boissonnault, S. M. Cohen, *Chem. Commun.* **2016**, *52*, 8585 – 8588; c) J. M. Roberts, B. M. Fini, A. A. Sarjeant, O. K. Farha, J. T. Hupp, K. A. Scheidt, *J. Am. Chem. Soc.* **2012**, *134*, 3334 – 3337; d) A. Broto-Ribas, C. Vignatti, A. Jimenez-Almarza, J. Luis-Barrera, Z. Dolatkhah, F. Gandara, I. Imaz, R. Mas-Balleste, J. Aleman, D. Maspoch, *Nano Res.* **2021**, *14*, 458 – 465; e) C. M. McGuirk, M. J. Katz, C. L. Stern, A. A. Sarjeant, J. T. Hupp, O. K. Farha, C. A. Mirkin, *J. Am. Chem. Soc.* **2015**, *137*, 919 – 925.

[14] a) M. Juhl, D. Tanner, *Chem. Soc. Rev.* **2009**, *38*, 2983 – 2992; b) X. Jiang, R. Wang, *Chem. Rev.* **2013**, *113*, 5515 – 5546; c) J. Kang, J. Rebek, Jr., *Nature* **1997**, *385*, 50 – 52.

[15] a) M. Yoshizawa, M. Tamura, M. Fujita, *Science* **2006**, *312*, 251 – 254; b) V. Mouarrawis, R. Plessius, J. I. van der Vlugt, J. N. H. Reek, *Front. Chem.* **2018**, *6*, 623; c) D. Samanta, S. Mukherjee, Y. P. Patil, P. S. Mukherjee, *Chem. Eur. J.* **2012**, *18*, 12322 – 12329.

[16] Y. Wu, H. Xu, X. Chen, J. Gao, D. Jiang, *Chem. Commun.* **2015**, *51*, 10096 – 10098.

[17] L. A. Hardegger, B. Kuhn, B. Spinnler, L. Anselm, R. Ecabert, M. Stihle, B. Gsell, R. Thoma, J. Diez, J. Benz, J. M. Plancher, G. Hartmann, D. W. Banner, W. Haap, F. Diederich, *Angew. Chem. Int. Ed.* **2011**, *50*, 314 – 318; *Angew. Chem.* **2011**, *123*, 329 – 334.

[18] a) D. Feng, H. L. Jiang, Y. P. Chen, Z. Y. Gu, Z. Wei, H. C. Zhou, *Inorg. Chem.* **2013**, *52*, 12661 – 12667; b) C. Koschnick, R. Staglich, T. Scholz, M. W. Terban, A. von Mankowski, G. Savasci, F. Binder, A. Schokel, M. Etter, J. Nuss, R. Siegel, L. S. Germann, C. Ochsenfeld, R. E. Dinnebier, J. Senker, B. V. Lotsch, *Nat. Commun.* **2021**, *12*, 3099.

[19] J. Blömker, W. Frey, *Z. Kristallogr. New Cryst. Struct.* **2000**, *215*, 267 – 268.

Manuscript received: September 1, 2021
Accepted manuscript online: September 8, 2021
Version of record online: October 1, 2021

